Complex strain partitioning patterns evaluated via triclinic transpression models. Kinematic analysis of the Valle de Abdalajís massif (Torcal shear zone, External Betics)

Patrones complejos de reparto de la deformación evaluados mediante modelos de transpresión triclínica. Análisis cinemático preliminar del macizo del Valle de Abdalajís (zona de cizalla del Torcal, zonas externas Béticas)

Manuel Díaz Azpiroz[1], Leticia Barcos[1], Inmaculada Expósito[1], Alejandro Jiménez[1], Juan Carlos Balanyá[1] and Carlos Fernández[2]

[1] Departamento de Sistemas Físicos, Químicos y Naturales. Universidad Pablo de Olavide. Crtra. Utrera, km 1, 41013 Sevilla, España.
mdiaazp@upo.es, lbarmur@upo.es, iexpram@upo.es, ajimbon@upo.es, jcbalrou@upo.es.
[2] Departamento de Geodinámica y Paleontología. Universidad de Huelva. Campus de El Carmen, 21071 Huelva, España.
fcarlos@uhu.es

ABSTRACT

Complex strain partitioning patterns are very common in the continental crust. They are often related to the kinematics of three-dimensional deformations and hence, can be analysed using transpression models. In this work, the strain partitioning pattern of the Valle de Abdalajís massif is evaluated with a model of triclinic transpression with oblique extrusion. Structures and kinematics are compared with the output of the model. We present preliminary results suggesting that the far-field vector responsible for bulk deformation at the studied area would be oriented NO75ºE-N144ºE, which is compatible with that of the neighbouring Torcal de Antequera massif. Bulk deformation affecting the Valle de Abdalajís massif was partitioned into strike-slip simple shear at the southern boundary and a triclinic transpressional component within the massif. Differences in strain partitioning pattern between these two massifs are unlikely related to flow partitioning.

Key-words: *External Betics, numerical modelling, shear zone, strain partitioning, triclinic transpression.*

RESUMEN

Los patrones complejos de reparto de la deformación son muy comunes en la corteza continental. Suelen relacionarse con la cinemática de deformaciones tridimensionales y pueden analizarse mediante modelos de transpresión. En este trabajo, se evalúa el patrón de reparto del macizo del Valle de Abdalajís con el modelo de transpresión triclínica con extrusión oblicua. Estos resultados sugieren que el vector responsable de la deformación de la zona estudiada tendría una orientación NO75ºE-N144ºE, rango que es compatible con la orientación del mismo vector para el vecino macizo del Torcal de Antequera. La deformación que afectó al macizo del Valle de Abdallajís se repartió entre una componente de cizalla simple lateral en el límite sur y una componente de transpresión triclínica en la parte interna del macizo. Es improbable que las diferencias en los patrones de reparto de ambos macizos se puedan relacionar con un reparto del flujo.

Palabras clave: *Zonas externas béticas, modelización numérica, zona de cizalla, reparto de la deformación, transpresión triclínica.*

Geogaceta, 56 (2014), 27-30.
ISSN (versión impresa): 0213-683X
ISSN (Internet): 2173-6545

Fecha de recepción: 31 de enero de 2014
Fecha de revisión: 29 de abril de 2014
Fecha de aceptación: 30 de mayo de 2014

Introduction

Crustal deformation is intrinsically heterogeneous and thus strain partitioning is a widespread feature within the crust (Jones *et al*., 2005). It can include two main situations: (1) several domains that accommodate the same bulk deformation with different sets of structures and/or (2) several domains and/or structures that accommodate different components of a single bulk deformation. A specific area can be affected simultaneously by these two partitioning situations, which usually take place at very different scales, finally resulting in very complex structural patterns.

Such complexity is usually related to intrinsic characteristics of the area affected by deformation, such as depth, or rock anisotropies among other (Carreras *et al*., 2013), but it can also be linked to the kinematics of deformation. This is one of the reasons why transpression models, which deal with three-dimensional deformation kinematics, have been specially used in ductile shear zones to decipher heterogeneous deformation and complex strain partitioning patterns (Davis and Titus, 2011). In contrast, despite its potential utility, these models have been seldom exploited to analyse upper crustal dominantly brittle deformation.

In this work, we employ the model of triclinic transpression with oblique extrusion (Fernández and Díaz-Azpiroz, 2009) to analyse the strain partitioning pattern of a shear zone developed under brittle-ductile conditions at the external Betics.

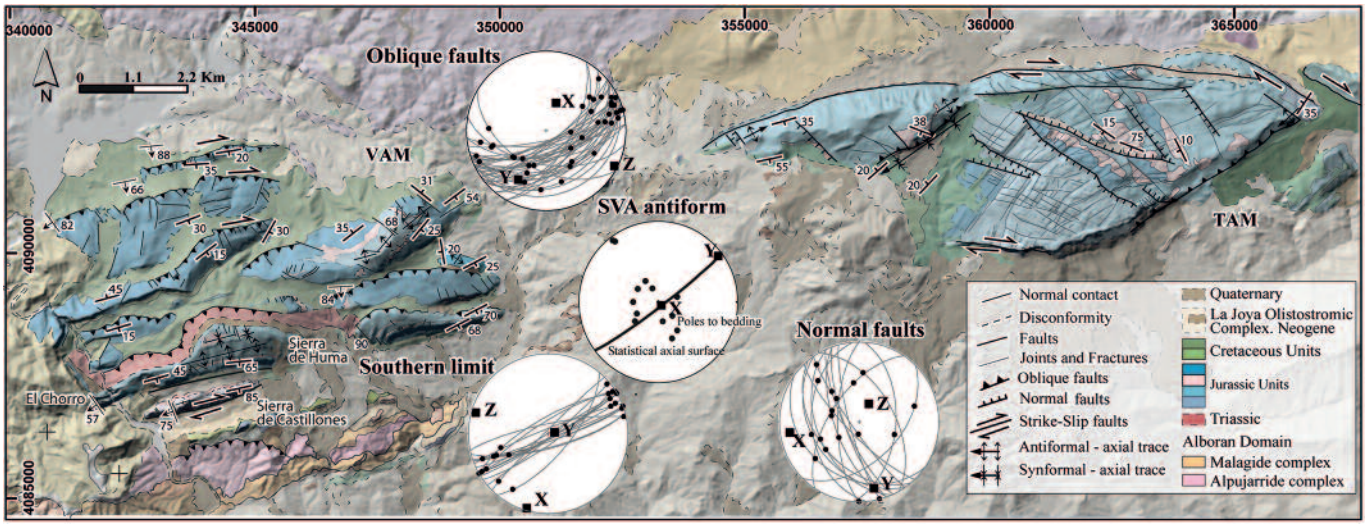

Fig. 1.- Structural map of the central sector of the Torcal shear zone with the Valle de Abdalajís and the Torcal de Antequera massifs (modified from Barcos *et al.*, 2011). Equal area, lower-hemisphere projections of fault planes and slickenlines, the Sierra de Abdalajís antiform axis and statistical axial surface, and orientation of the main finite strain axes deduced in each case.

Fig. 1.- Mapa estructural del sector central de la zona de cizalla del Torcal con los macizos del Valle de Abdalajís y del Torcal de Antequera (modificado de Barcos* et al.*, 2011). Proyecciones equiareales (hemisferio inferior) de planos y lineaciones, el eje y plano axial estadístico del antiforme de la Sierra de Abdalajís, así como la orientación de los ejes de deformación finita deducidos en cada caso.

Structure of the Valle de Abdalajís massif

The Torcal shear zone (TSZ) is roughly E-W oriented and defines a recess zone connecting two second-order arcs within the northern branch of the Gibraltar Arc (Barcos *et al.*, 2011). Its central sector presents two main massifs where Subbetic units of the Southiberian domain crop out (Fig. 1): the Valle de Abdalajís massif (VAM) and the Torcal de Antequera massif (TAM).

The internal structure of the VAM is essentially defined by (1) roughly SW-NE trending folds with axes shallowly plunging towards the NE; (2) SSE dipping oblique faults with a reverse displacement and significant amounts of lateral, mainly dextral and minor sinistral, motion; and (3) normal faults accommodating extension subparallel to the direction of folds and oblique faults. In addition, the southern boundary of the VAM is a mainly dextral strike-slip fault zone with negligible amounts of dip-slip simple shear or coaxial deformation.

Kinematic analysis

Methodology

The orientations of the finite strain ellipsoid have been estimated separately for the four different structure types. In the case of folds, the X-axis has been located parallel to the facing direction whereas the Y-axis tracks the fold axis (e.g., Jones *et al.*, 2004). In the other cases, fault-slip data have been analysed via the Moment Tensor Summation at Faultkin software (Allmendinger *et al.*, 1994) to obtain the orientation of the corresponding incremental strain tensor (Marrett and Allmendinger, 1990), which can be used as a proxy for the finite strain ellipsoid if the total extension is lower than 60 %.

Kinematic data obtained from the internal part of the VAM (that is, excluding the strike-slip fault constituting the southern boundary) are compared with the model of triclinic transpression with oblique extrusion (Fernández and Díaz-Azpiroz, 2009). This model assumes (1) a tabular shear zone with slip occurring along its boundaries; and (2) homogeneous, isochoric and steady deformation. To model homogeneous deformation, each structure type (oblique faults and folds stretched by normal faults) is analysed individually.

The main input parameters of the model are: (1) transpression obliquity (ϕ), defined as the angle between the simple shearing direction and the strike of the shear zone; (2) extrusion obliquity (υ), which is the angle between the extrusion direction of the coaxial component of deformation and the dip direction of the shear zone; (3) the kinematic vorticity number (W_k), a measure of the ratio between the simple shearing ($\dot{\gamma}$) and the coaxial component of deformation ($\dot{\varepsilon}$); and the amount of finite strain (S). In this case, we use previous results from the neighbouring TAM (Díaz-Azpiroz *et al.*, 2014) to constrain S between 0.05 and 0.4.

For this study, it is relevant to compare these results with those obtained from the TAM as well as with tectonic plates velocity vectors deduced for the western Mediterranean area. To achieve such comparison, the obtained kinematic (internal) parameters are used to estimate geometrical (external) parameters (Schulmann *et al.*, 2003). The angle of oblique convergence (α) is measured between the strike of the shear zone and the azimuth of the far-field vector ($\vec{F}_d$), which defines the relative displacement of the undeformed blocks on both sides of the shear zone (Jones *et al.*, 2004). The azimuth of $\vec{F}_d$ coincides with the strike of the vorticity normal section (VNS), whose orientation can be estimated from ϕ and W_k (Jiang and Williams, 1998).

The comparison between the natural case and the model is carried out following a standard procedure (Díaz-Azpiroz *et al.*, 2014) with three steps: (1) ϕ and υ values are constrained from geological observations; (2) the orientations of the finite strain ellipsoid obtained from the two types of structures within the internal part of the VAM (oblique faults and folds+normal faults) are compared with results (λ_1, λ_2, λ_3) from the model (Fig. 2A and B); (3) the angle of oblique convergence (α) is calculated from the orientation of the shear zone

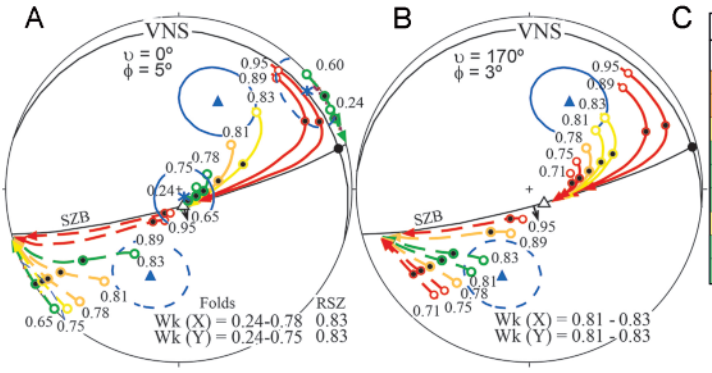

C

F + NF								OF			
ϕ	W_k	α_{min}	α_{Max}	ϕ	W_k	α_{min}	α_{Max}	ϕ	W_k	α_{min}	α_{Max}
2	0.6	14	34	5	0.71	27	32	2	0.83	14	19
2	0.65	14	31	5	0.75	24	32	3	0.78	21	22
2	0.71	14	27	5	0.78	22	32	3	0.81	20	21
2	0.75	14	24	10	0.24	52	65	3	0.83	19	21
2	0.78	14	22	10	0.45	45	52	3	0.89	15	21
2	0.81	14	20	10	0.6	34	52	5	0.83	19	32
5	0.45	32	45	10	0.65	32	52				
5	0.6	32	34	15	0.24	63	65				
5	0.65	31	32	20	0.24	65	69				

Fig. 2.- Procedure followed to compare the kinematic data of the VAM with the model of triclinic transpression with oblique extrusion. (A) and (B) Two examples ($\upsilon = 0°/\phi = 5°$; $\upsilon = 170°/\phi = 3°$) of step 2: equal area, lower hemisphere plots with the orientation of X and Y axes of the strain ellipsoid (in blue, with a 95 % confidence cone) deduced from oblique faults (triangles) and folds (asterisks). This is compared with the evolution with increasing finite strain of the theoretical loci of λ_1 (solid) and λ_2 (dashed) obtained from the model, for different W_k values (in normal font for λ_1 and in italic for λ_2). Along each arrow, the most likely finite strain interval (see the text) is marked by a white (S = 0.05) and a black (S = 0.4) circle. W_k ranges yielding fair to good fits in each case are shown. SZB: Shear Zone Boundary (black arrow: dip direction); VNS: Vorticity Normal Section; black circle: simple shearing; white triangle: extrusion direction due to the coaxial component of deformation. (C) Results of step 3: Comparison of α values obtained from combinations of ϕ and W_k values yielding any fit in step 2. Colour code (colour version on web) indicates the quality of fit: good (green), fair (yellow), poor (orange) and absent (red).

Fig. 2.- Procedimiento seguido para comparar los datos cinemáticos del VAM con el modelo de transpresión triclínica con extrusión oblicua. (A) y (B) Dos ejemplos ($\upsilon = 0°/\phi = 5°$; $\upsilon = 170°/\phi = 3°$) del paso 2: proyecciones equiareales (hemisferio inferior) con las orientaciones de los ejes X e Y del elipsoide de deformación (en azul, con un cono de confianza del 95 %) deducidas de las fallas oblicua (triángulos) y pliegues (asteriscos). Estas se comparan con la evolución, con el incremento de la deformación finita, de la orientación de λ_1 (línea sólida) y λ_2 (línea a trazos) obtenida del modelo, para valores distintos de W_k (letra normal para λ_1 y cursiva para λ_2). A lo largo de cada trayectoria, se marca el intervalo de deformación finita más probable (véase el texto) mediante sendos círculos (blanco para S = 0.05, negro para S = 0.4). En cada caso, se muestran los rangos de Wk que generan un ajuste válido o bueno. SZB: límites de la zona de cizalla (flecha negra: dirección de buzamiento); VNS: sección de máxima vorticidad; círculo negro: dirección de cizalla simple; triángulo blanco: dirección de extrusión del componente coaxial. (C) Resultados del paso 3: Comparación de los valores de α obtenido con combinaciones de ϕ y W_k que hayan producido algún ajuste en el paso 2. El código de colores indica la calidad del ajuste: bueno (verde), válido (amarillo), pobre (naranja), ninguno (rojo). (ver figura en color en la página web).

and using, independently, the values of the kinematic parameters (ϕ and W_k) deduced previously. Only those combinations of ϕ/W_k values that resemble the loci of both the X and the Y axes are tested through step 3 (Fig. 2C). In this step, the deviations in α results obtained from ϕ and W_k are evaluated. If after applying this procedure there are no results that satisfy the data from the natural case, the process should start again from the first step reconsidering the initial kinematic parameters.

Results

The orientation of the finite strain ellipsoid deduced for each structure type within the VAM (oblique faults and folds+normal faults) is shown in figure 1. The orientation of these structures and that of the finite strain ellipsoid deduced from them are compatible with dextral transpression. The deformation accommodated by normal faults produced minor fold-axis parallel extension, which is typical of transpressional systems (e.g., Titus *et al.*, 2007). Note that the X and Z axes deduced from normal faults are subparallel, respectively, to the Y and X axes-axis deduced from folds. This would modify the final shape of the folds strain ellipsoid to an apparent flattening type but would not produce significant modifications in its orientation. These results are compared with the triclinic transpression model.

Step 1: In the internal part of the VAM, the simple shear component is partitioned between folds+normal faults and oblique faults. Fold-axis parallel stretching and the gentle plunging of most slickenlines on oblique fault planes, suggest ϕ value is low (<20°). Also, there are no evidences in the VAM suggesting oblique extrusion. Therefore, in this preliminary data-set, υ angle has been considered 0°.

Step 2: The orientations of both the X and Y axes of the finite strain ellipsoid deduced for the folds can be resembled by the model with a wide combination of ϕ (2-20°) and W_k (0.24-0.81) values. In contrast, only ϕ = 20° and W_k = 0.83-0.89 yield a good or fair fit with the X and Y axes obtained from the oblique faults (Fig. 2A).

Step 3: The combinations of ϕ/W_k values that best meet the three conditions here proposed (X and Y axes, and deviation of angle α) for the folds+normal faults are: 5°/0.6-0.65, 10°/0.45 and 15-20°/0.24. Taking into account the orientation of the VAM (N075°E/82°S), the resulting F_d would be oriented between N095°E and N144°E (Table I, Fig. 3). In contrast, there is no combination of ϕ/W_k values that would explain satisfactorily the oblique faults (Fig. 2C) and thus, the range of possible kinematic parameters should be reconsidered.

υ	ϕ	W_k	α	$\vec{F}_d$
F+NF				
0	2	0.6-0-71		
0	2	0.75-0.81	20-24	095-099
0	5	0.45		
0	5	0.6-0.75	24-34	099-109
0	5	0.78		
0	10	0.24		
0	10	0.45	45-52	120-127
0	10	0.6-0.65		
0	15	0.24	63-65	138-140
0	20	0.24	63-69	138-144
OF				
0	5	0.83		
170	2-4	0.81-0.83	14-27	089-102
170	5	0.81-0.83		

Table I.- Summary of kinematic and geometrical parameters deduced for the structures in the internal VAM.

Tabla I.- Resumen de los parámetros cinemáticos y geométricos deducidos para las estructuras de la parte interna del VAM.

In this preliminary stage of the study, a possible explanation for the oblique faults of the VAM can only be achieved qualitatively. One possibility would be a deviation

of the extrusion direction with respect to the dip direction. An extrusion obliquity of 10º towards the ENE ($\upsilon = 170º$) would force λ_1 obtained from low W_k values (< 0.85) to plot closer to the simple shear direction (Fernández and Díaz-Azpiroz, 2009). Therefore, the loci of λ_1 from W_k = 0.78-0.85 would approach the orientation of the X-axis from oblique faults (Fig. 2B). Combination of ϕ/W_k values of 2-4º/0.81-0.83 would produce deviations smaller than 10º in the resulting α values (Fig. 2C) with F_d oriented NO89ºE-N102ºE (Table I, Fig. 3).

Discussion

Assuming all the structures analysed here correspond to a single deformational event, our results suggest that the bulk deformation affecting the VAM was partitioned into a dextral strike-slip simple shear fault constituting the southern boundary and a wider internal domain accommodating triclinic transpression (ϕ = 2-20º, $W_k \approx$ 0.7-0.8). This deformation would have been accommodated by folds stretched along-axis via normal faults (ϕ = 2-20º, W_k = 0.24-0.81) and oblique faults with right and left lateral minor displacement (ϕ = 2-4º, W_k = 0.81-0.83) and an oblique NW-upward directed extrusion.

This discrete strain partitioning pattern differs from that observed in the TAM, which presents two narrow outer domains that accommodate simple shear dominated dextral transpression, and a wider inner domain deformed by coaxially dominated triclinic transpression (Barcos *et al.*, 2011).

In the previous section, we have shown that the F_d responsible for the folds and the oblique faults of the VAM is oriented NO95ºE-N144ºE and NO89ºE-N102ºE, respectively (Table I). On its turn, the F_d responsible for the deformation at the VAM southern boundary is likely subparallel to the strike of the shear zone boundary (NO75ºE). Therefore, the F_d that would account for the bulk strain accommodated by the VAM would be located between NO75ºE and N144ºE (Fig. 3). The F_d deduced for the TAM (Díaz-Azpiroz *et al.*, 2014) is oriented NO99ºE-N118ºE, which is located within the orientation range deduced for the VAM. The imprecision of the latter would permit differences in F_d orientation between both massifs of up to 45º. However, the central position of the TAM F_d within the VAM F_d span (Fig. 3) suggests that a single F_d could have been responsible for the deformation observed in both massifs. Therefore, the bulk deformation affecting both massifs would have been very similar and would probably represent the bulk deformation for the Torcal shear zone. In any case, the possible differences in F_d orientation and bulk deformation between the TAM and the VAM would have unlikely produced the contrasting strain partitioning patterns shown by these two massifs. Hence, other causes should be invoked.

Conclusions

In this work, the structural pattern and the kinematics of the Valle de Abdalajís massif (VAM) are compared with a model of triclinic transpression. The main conclusions are: (1) Bulk deformation affecting the VAM was dextral triclinic transpression, related to a far-field vector oriented between NO75ºE and N144ºE. (2) This was partitioned into a dextral strike-slip fault constituting the southern boundary of the VAM and a wider internal domain, which accommodated triclinic transpression via folds with axis-parallel extension and oblique faults. (3) The orientation of the far-field vector deduced for the neighbouring Torcal de Antequera massif is compatible with the orientation range of the VAM far-field vector. (4) Contrasting strain partitioning patterns observed along strike in different massifs of the Torcal shear zone are unlikely related to differences in the orientation of their respective far-field vectors.

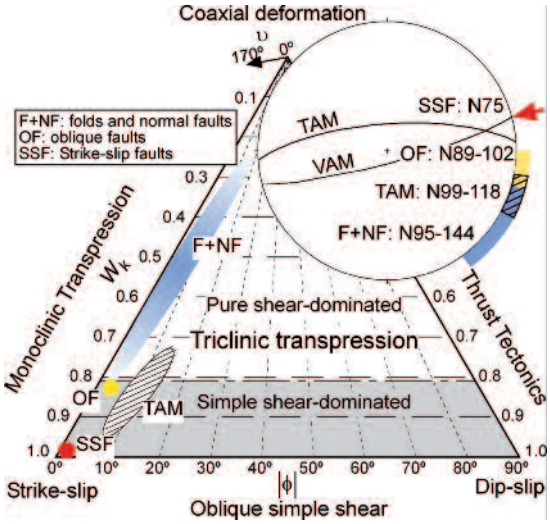

Fig. 3.- Strain partitioning within the VAM in a strain triangle based on that of Jones *et al.* (2004), with contour lines for ϕ and W_k, and υ values of 0º and 170º. The pole figure shows the average orientations of the VAM and the TAM and the possible range of the azimuth of F_d for different domains of the TSZ.

Fig. 3.- Reparto de la deformación en el VAM representado en un triángulo de strain basado en el de Jones* et al. *(2004) con líneas de contorno para ϕ and W_k, y valores de υ de 0º y 170º. El estereograma muestra las orientaciones medias del VAM y el TAM, así como el rango posible de orientaciones de F_d para distintos dominios de la TSZ.

Acknowledgments

Financial support from Projects CGL2009-11384/BTE and TOPO-IBERIA CONSOLIDER-INGENIO 2010-CSD2006-0041. Reviews by A. Casas and E. Druguet and editorial work by I. Arenillas are gratefully acknowledged.

References

Allmendinger, R.W., Marrett, R.A. and Cladouhos, T. (1994). *A Program for Analyzing Fault–slip Data on a Macintosh Computer*, Absoft Corp.

Barcos, L., Díaz Azpiroz, M., Balanyá, J.C. and Expósito, I. (2011). *Geogaceta* 50, 31-34.

Carreras, J., Druguet, E. and Cosgrove, J. W. (2013). *Journal of Structural Geology* 50, 7-21.

Davis, J.R. and Titus, S.J. (2011). *Journal of Structural Geology* 33, 1043-1062.

Díaz-Azpiroz, M., Barcos, L., Balanyá, J.C., Fernández, C., Expósito, I. and Czeck, D.M. (2014). *Journal of Structural Geology* 68, 316-336.

Fernández, C. and Díaz-Azpiroz, M. (2009). *Journal of Structural Geology* 31, 1255-1269.

Jiang, D. and Williams, P.F. (1998). *Journal of Structural Geology* 20, 1105-1120.

Jones, R.R., Holdsworth, R.E., Clegg, P., McCaffrey, K. and Tavarnelli, E. (2004). *Journal of Structural Geology* 26, 1531-1548.

Jones, R.R., Holdsworth, R.E., McCaffrey, K.J.W., Clegg, P. and Tavarnelli, E. (2005). *Journal of Structural Geology* 27, 1190-1204.

Marrett, R. and Allmendinger, R.W. (1990). *Journal of Structural Geology* 12, 973-986.

Schulmann, K., Thompson, A.B., Lexa, O. and Ježek, J. (2003). *Journal of Geophysical Research* 108 (B1). ETG 6-1 – ETG 6-15.

Titus, S.J., Housen, B. and Tikoff, B. (2007). *Journal of Structural Geology* 29, 961–982.